

## Comparison of *UBVR* Photometry of Giant HII Regions in the Galaxy NGC 628 with a Detailed Grid of Evolutionary Models for Star Clusters

V. V. Bruevich<sup>1</sup>, A. S. Gusev<sup>1</sup>, O. V. Ezhkova<sup>1</sup>, F. Kh. Sakhibov<sup>2,3</sup>, and M. A. Smirnov<sup>†4</sup>

<sup>1</sup>*Sternberg Astronomical Institute, Universitetskii pr. 13, Moscow, 119992 Russia*

<sup>2</sup>*Giessen–Friedberg University of Applied Sciences, Wilhelm-Leuschner-Strasse 13, Friedberg, 61169 Germany*

<sup>3</sup>*Institute of Astrophysics, Academy of Sciences of Tajikistan, ul. Bukhoro 22, Dushanbe, 734042 Tajikistan*

<sup>4</sup>*Institute of Astronomy, ul. Pyatnitskaya 48, Moscow, 119017 Russia*

Received April 10, 2006; in final form, October 12, 2006

**Abstract**—We present the results of *UBVRI* CCD photometry of giant HII regions in the spiral galaxy NGC 628, acquired with the 1.5 m telescope of the Mt. Maidanak Observatory (Uzbekistan) with an angular resolution better than 1". We estimate the ages and interstellar extinctions of these regions and identify the acting star-formation mode by comparing the observed color indices with a detailed grid of evolutionary models covering the entire range of parameters of the initial mass function and of ages of the young star-formation complexes, and taking into account two star-formation modes. We find a radial gradient of the interstellar extinction in NGC 628, which is consistent with the radial abundance gradient found earlier by other authors from independent spectrophotometry. Our age estimates agree with abundance estimates from independent observations.

PACS numbers : 95.75.De, 95.85.Kr, 98.20.Fk, 98.35.Ac, 98.35.Hj, 98.38.Gt, 98.52.Nr

DOI: 10.1134/S1063772907030043

### 1. INTRODUCTION

This paper is devoted to a study of young star-formation complexes (SFCs), seen as giant HII regions, in the spiral galaxy NGC 628 based on *UBVR* photometry. The late-ScI giant spiral galaxy NGC 628 is one of only a few very well studied galaxies. Observational studies of this galaxy include the multicolor photographic photometry of giant HII regions [1]; multicolor *UBVRJ* surface photometry of the stellar disk and analysis of its morphology [2]; a complete H $\alpha$  photometric survey of 583 HII regions [3]; a detailed two-dimensional radial-velocity field derived from aperture synthesis observations for the optically visible part of the galaxy [4] and then extended to the outer part, visible in the radio [5]; and a complete spectrophotometric survey of 130 giant HII regions [6]. The main optical characteristics of NGC 628 can be found in the papers cited above, as well as [7–9]. Following [10], we take the distance to NGC 628 to be 7.2 kpc. We derived the position angle of the major axis, PA = 25°, and the inclination of the galactic disk,  $i = 7^\circ$ , in our earlier paper [11], based on a Fourier analysis of the spatial distribution of the radial velocities of the gas in the disk.

In our study of the physical characteristics of star clusters based on multicolor photometry, we will use the method developed in our earlier papers [12, 13]. The problem at hand—determining the initial mass function (IMF), age, star-formation rate and star-formation mode from the known spectral energy distribution of a star cluster—can be reduced to searching for the minimum of the deviation functional. The deviation functional is a numerical function relating each evolutionary model to a number describing the total deviation of the observed photometric data from the model. We discuss the difference between this approach and current classical techniques of evolutionary population synthesis in our earlier papers [14, 15]. Paper [14] also models the solution of the problem at hand under various conditions.

Along with multicolor photometry of the stellar continuum, spectroscopy and spectrophotometry in gas emission lines, which contain information about the internal extinction and the chemical compositions of the SFCs represent necessary observational data for the present study. Thus, the main criterion for our choice of objects for the multicolor photometric observations was the availability of emission-line spectrophotometry for these objects. Belley and Roy [6] present spectrophotometric observations in

<sup>†</sup>Deceased.

hydrogen, nitrogen, and oxygen emission lines for 130 giant HII regions in the spiral galaxy NGC 628. It is the young star clusters creating these giant regions of ionized hydrogen that are the objects of the present study. We aim here to determine the physical characteristics of the star formation (IMF and star-formation history) by analyzing our multicolor photometric data for these objects using an appropriate deviation functional.

This paper presents the results of broadband *UBVR* photometry of 127 giant regions of ionized hydrogen (HII regions) in the spiral galaxy NGC 628, which were earlier studied using spectrophotometric observations in emission lines of hydrogen, nitrogen, and oxygen [6]. This combination of observational characteristics was compared to a detailed grid of evolutionary models, computed at the Institute of Astronomy of the Russian Academy of Sciences (INASAN) [16] using deviation functionals. For 57 star-formation complexes, we were able to express the photometric data in terms of a star-formation history (ages and star-formation modes).

The paper has 10 sections, including an Introduction and Conclusion. Section 2 presents our broadband *UBVRI* CCD photometry of SFCs in NGC 628 using the 1.5 m telescope of the Mt. Maidanak Observatory (Uzbekistan). Section 3 presents the characteristics of the spectrophotometric data of [6]. Section 4 compares the observed colors to the grid of evolution models using deviation functionals. Section 5 presents our estimates of the interstellar extinction for the SFCs in NGC 628. Section 6 considered how the age–extinction effect influences the results. We study the radial extinction gradient in NGC 628 in Section 7. The ages of the SFCs in NGC 628 are discussed in Section 8. Section 9 compares theoretical Lyman-continuum fluxes to measured fluxes in hydrogen emission lines emitted by SFCs in NGC 628. Our main conclusions are summarized in Section 10.

## 2. *UBVRI* PHOTOMETRY OF THE SFCs IN NGC 628

This section presents the results of our multicolor photometry of 127 giant HII regions in the spiral galaxy NGC 628. We obtained these data for those HII regions for which Belley and Roy [6] obtained spectrophotometric data in hydrogen, nitrogen, and oxygen emission lines and determined their interstellar extinctions and chemical compositions.

The observations in the *U*, *B*, *V*, *R*, and *I* bands were obtained by V.V. Bruevich and O.V. Ezhkova in October 2002 with the 1.5 m (12 m focal length) telescope of the Mt. Maidanak Observatory (Institute of Astronomy, Academy of Sciences, Republic

of Uzbekistan) using an SIT-2000 CCD camera. With the *U*, *B*, *V*, *R*, and *I* broadband filters, the CCD chip reproduces a photometric system close to the standard Johnson–Cousins *UBVRI* system. Information on the filters used for our observations is published in [17]. The camera is cooled with liquid nitrogen. The chip has  $2000 \times 800$  pixels, providing an  $8.9' \times 3.6'$  field of view with an image scale of  $0.267''/\text{pixel} \times 0.267''$  per pixel. Since the angular size of NGC 628 is larger than the field of view, we obtained separate images for the galaxy's northern and southern parts. A log of our observations is given in Table 1.

Further data reduction was carried out at the Sternberg Astronomical Institute (Moscow State University) using the standard procedure implemented in the ESO–MIDAS image-reduction package. The main stages of the reduction include determining and applying a bias and flat field; removing cosmic-ray traces; determining the sky background and subtracting it from each image; assembling the images of the galaxy using reference stars; summing the galaxy images in the same filter; normalizing and joining the northern and southern parts of the galaxy; carrying out the photometric calibration, i.e. reducing the data from the instrumental photometric system to the standard Johnson–Cousins system and correcting for the air mass (using the derived color equations and the results of the aperture photometry of the galaxy). We derived the color equations and corrected for atmospheric extinction using observations of stars from the Landolt fields [18] SA 92, SA 110, SA 111, and SA 113, acquired on the same nights in the *U*, *B*, *V*, *R*, and *I* filters at air masses of  $M(z) \equiv \sec z = 1.28\text{--}1.57$ . *UBVRI* photometry was obtained for 17 stars, with fluxes for different  $M(z)$  values measured for 13 of them. The resulting instrumental *ubvri* system was close to the standard Johnson–Cousins *UBVRI* photometric system with an accuracy better than  $0.04^m$  in the *B*, *V*, *R*, and *I* bands and better than  $0.11^m$  in the *U* band [19]. In addition, we compared the data for the galaxy with the results of aperture photometry (from the HyperLEDA electronic catalog). The accuracy of the photometric reduction and the zero-point error are within the uncertainties of the derived color equations.

For an adopted distance to NGC 628 of 7.2 Mpc, the scale of our images is 34.9 pc/arcsecond (9.31 pc/pixel).

We identified the SFCs with the HII regions from [3, 6]. Note that our coordinate grid coincides with that of Kennicutt and Hodge [3] and is systematically shifted with respect to that of Belley and Roy [6] (Fig. 1). Altogether, we identified 127 SFCs of the 132 studied in [6]. Three SFCs (Nos. 1, 2, and

**Table 1.** Log of observations

Date	Region of the galaxy	Filter	Exposure times, s	Air mass	Seeing
Sept. 11, 2002	S	<i>U</i>	4 × 300	1.09	1.18''
	N	<i>U</i>	4 × 300	1.11	1.17
	S	<i>B</i>	2 × 300	1.09	0.95
	N	<i>B</i>	2 × 300	1.14	0.97
	S	<i>V</i>	2 × 240	1.09	0.93
	N	<i>V</i>	2 × 240	1.16	0.95
	S	<i>R</i>	2 × 150	1.10	0.88
	N	<i>R</i>	2 × 150	1.10	0.85
	N	<i>R</i>	6 × 10	1.15	1.00
	S	<i>I</i>	2 × 120	1.10	0.78
Sept. 30, 2002	N	<i>I</i>	2 × 120	1.10	0.77
	S	<i>U</i>	4 × 300	1.13	0.89
	N	<i>U</i>	4 × 300	1.25	1.01
	S	<i>B</i>	2 × 300	1.16	0.91
	N	<i>B</i>	2 × 300	1.30	1.12
	S	<i>V</i>	2 × 240	1.17	0.85
	N	<i>V</i>	2 × 240	1.33	0.97
	S	<i>R</i>	2 × 150	1.11	0.77
	N	<i>R</i>	2 × 150	1.20	0.69
	S	<i>I</i>	2 × 120	1.12	0.74
N	<i>I</i>	2 × 120	1.21	0.64	

96 in [6]) are outside the field of view of our images. Two SFCs (Nos. 23 and 76) are missing in [6]. The observed color indices, sizes, and positions of the SFCs are collected in Table 2 (due to its large volume, Table 2 is published in full form only electronically, see <http://lnfm1.sai.msu.ru/gusev/n628t3.dat>). Belley and Roy [6] did not distinguish between isolated SFCs, with typical sizes about 70 pc, and compound multi-component SFCs, with typical sizes about 200 pc. We subdivided the compound SFCs into components, complexes with star-like brightness profiles. The numbers of these complexes in the first column of Table 2 contain additional letters: “a,” “b,” “c,” “d,” etc. We should make clear right from the start that a comparison with the evolutionary models was made only for the 127 objects studied in [6]; multi-component objects listed by Belley and Roy [6] as single objects are considered here to be single star-formation complexes. In our subsequent analysis, we will discuss only those objects that do not have an additional index in the first column of Table 2.

The remarks in Table 2 indicate the morphological features of some of the SFCs.

The first row of columns in Table 2 contain (1) ordinal number of the SFC, (2) number of the SFC from [6], (3) number of the SFC from the list in Kennicutt and Hodge [3], (4) coordinates in arcseconds from the galaxy’s center, (5) the deprojected distance to the galaxy’s center in kpc, (6) the SFC’s characteristic size in pc, and (7) remarks. We calculated the deprojected distances to the center of NGC 628 using the major-axis position angle  $PA = 25^\circ$  and disk inclination  $i = 7^\circ$  [11]. We took the geometric average of the SFC’s major and minor axes for the SFC’s characteristic size,  $d: d = \sqrt{d_{\max} \times d_{\min}}$ . We measured  $d_{\max}$  and  $d_{\min}$  from the radial  $V$  profiles at the half-maximum brightness level (FWHM). The uncertainty in  $d$  is about 20 pc. The following SFC properties are indicated in the remarks: d = double, t = triple, ring = ring-shaped, dif = diffuse, sep = separated, pSFR = brightest part (core) of an extended star-forming zone (region). The Roman nu-

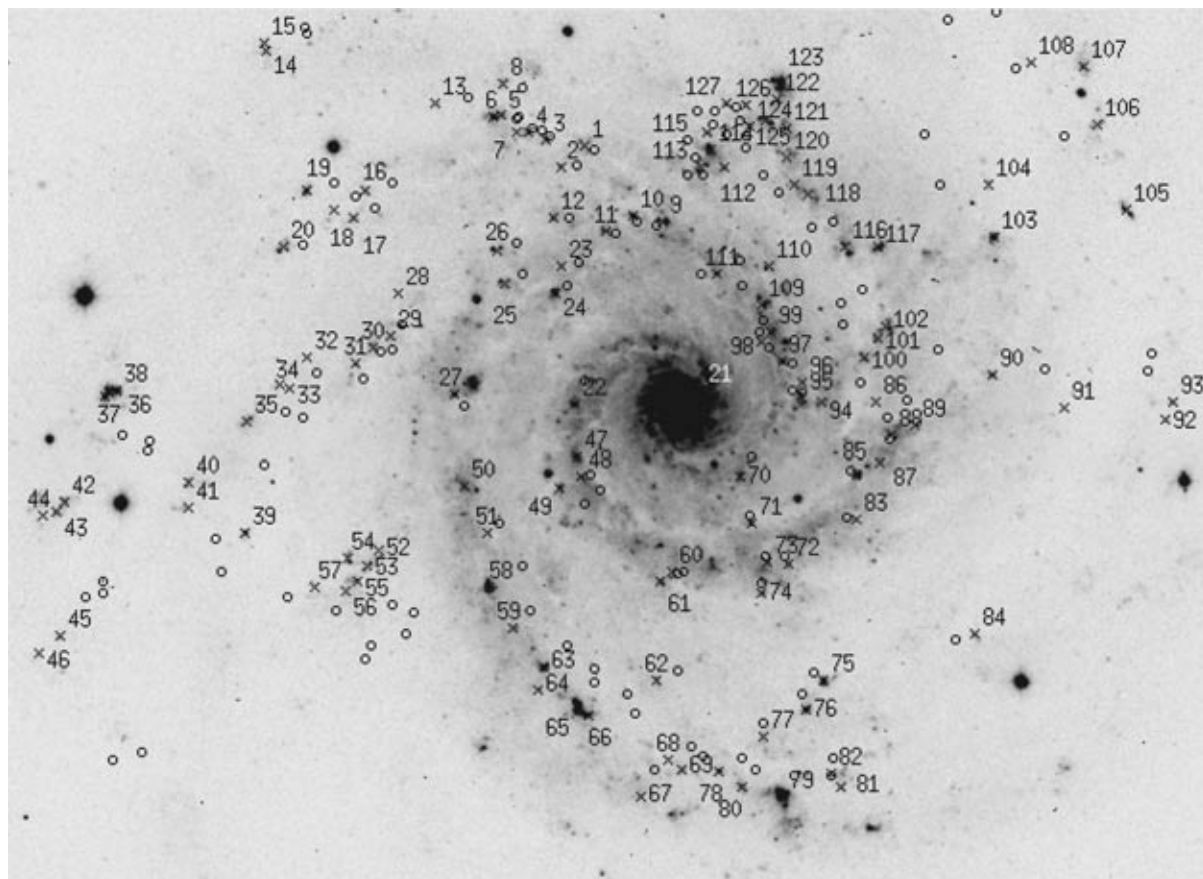


**Fig. 1.** *B* image of NGC 628 and positions of the galaxy's SFCs according to the coordinates of Belley and Roy [6] (circles) and our own data (crosses). The numbers of the SFCs from Table 2 are indicated. The image is  $8.26' \times 6.00'$  in size. North is upward and east to the left.

merals I–X designate 10 star-formation zones that were subdivided into individual SFCs in [6]. Thus, keeping the numbers proposed in [6], we subdivide the objects into two hierarchy types: compound objects, with characteristic sizes of about 200 pc (for example, Nos. I, 9), and single objects, with characteristic sizes of about 70 pc (for example, Nos. 1a–1d, 2, 3).

The second row of columns in Table 2 contain the photometric characteristics of the SFCs—(2)  $m_B$  and (3–6) the color indices  $U-B$ ,  $B-V$ ,  $V-R$ , and  $V-I$  with their uncertainties. None of the data were corrected for extinction in our Galaxy (see below). All measurements were made in round apertures, and the light from the surrounding background was subtracted from the light coming from the region occupied by the SFC. For the  $m_B$  measurements, the aperture used corresponded to the sum of  $d_{\max}$  and the seeing (assumed to be  $1''$  in the *B* band). The aperture used for the color-index measurements was  $d_{\max}$ . The apertures for measuring the SFC luminosities were chosen so that the aperture contained all the light from the complex. The  $m_B$  magnitudes measured for SFCs in high-density star-forming regions are real-

istic lower limits for their luminosities. The apertures used to measure the color indices were smaller, since we are interested in the spectral energy distribution in the brightest and the most active parts of the SFCs. The use of larger apertures would increase the uncertainties of the measured color indices and permit light from older stars to enter the aperture. The photometric errors in Table 2 correspond to the uncertainties in the aperture photometry. The uncertainties in the photometric calibration for NGC 628, described above, were not included here.

### 3. SPECTROPHOTOMETRY OF SFCs IN NGC 628

Belley and Roy [6] presented spectrophotometric data for 130 giant HII regions in the spiral galaxy NGC 628 in hydrogen, nitrogen, and oxygen lines. They used these observations to derive several physical parameters, including those of interest for us: the interstellar extinction in the Balmer hydrogen lines and metallicity estimates for these objects. Using their metallicity estimates for 130 objects distributed

**Table 2.** SFC parameters

No.	No. from [6] $m(B)$	No. from [3] $U-B$	$X, Y$ , arcsec $B-V$	$r$ , kpc $V-R$	$d$ , pc $V-I$	Remarks*
1	3	121+122	39.0E, 106.9N	3.97	230	
	$18.89 \pm 0.01$	$-0.35 \pm 0.02$	$0.18 \pm 0.02$	$0.36 \pm 0.02$	$0.35 \pm 0.02$	
1a			40.3E, 108.8N	4.05	65	
	$20.81 \pm 0.02$	$-0.61 \pm 0.02$	$0.02 \pm 0.04$	$0.26 \pm 0.04$	$-0.10 \pm 0.06$	
1b			38.5E, 106.9N	3.97 (!)	105	d
	$20.50 \pm 0.02$	$-0.52 \pm 0.02$	$0.10 \pm 0.03$	$0.33 \pm 0.03$	$0.24 \pm 0.04$	
1c			37.4E, 104.2N	3.87	70	
	$21.07 \pm 0.02$	$-0.20 \pm 0.03$	$0.36 \pm 0.03$	$0.30 \pm 0.03$	$0.44 \pm 0.03$	
1d			36.6E, 110.4N	4.06	70	
	$21.44 \pm 0.03$	$-0.25 \pm 0.04$	$0.36 \pm 0.04$	$0.21 \pm 0.05$	$0.35 \pm 0.05$	
2	4	126+127	48.6E, 98.4N	3.83	50	
	$20.56 \pm 0.01$	$-0.88 \pm 0.02$	$-0.02 \pm 0.02$	$0.46 \pm 0.02$	$-0.11 \pm 0.05$	
3	5	125	54.5E, 109.0N	4.25	120	t, ring
	$20.81 \pm 0.03$	$-0.34 \pm 0.04$	$0.24 \pm 0.05$	$0.15 \pm 0.05$	$0.17 \pm 0.06$	
4	6	129	61.9E, 112.2N	4.48 (!)	80	pSFR
	$20.12 \pm 0.01$	$-0.92 \pm 0.01$	$0.16 \pm 0.02$	$0.78 \pm 0.02$	$0.22 \pm 0.03$	
5	7	133+133a	72.9E, 119.7N	4.90	50	I
	$20.19 \pm 0.01$	$-0.70 \pm 0.01$	$0.08 \pm 0.02$	$0.44 \pm 0.02$	$0.14 \pm 0.03$	
6	8	134+135	76.1E, 119.2N	4.94	50	I
	$19.05 \pm 0.01$	$-0.52 \pm 0.01$	$0.19 \pm 0.01$	$0.18 \pm 0.01$	$0.20 \pm 0.01$	

\* The notation used in this column is explained in the text.

across the entire optical disk of the galaxy, Belley and Roy [6] demonstrated the presence of a chemical-composition gradient in the galactic disk.

We used the empirical calibrations of [20, 21] to calculate the abundance parameter  $Z$  for the 127 HII regions based on the relative intensities of the oxygen and nitrogen lines measured in [6]. Our comparison of the data given in [6] with the results of other authors reveals the following differences.

First, Belley and Roy [6] derived the sizes of the HII regions from measurements of their images in  $H\alpha$  emission. The  $H\alpha$  images were obtained with a narrow filter,  $\Delta\lambda = 11 \text{ \AA}$ , and so also include faint outer regions of the SFCs. The sizes of the HII regions measured in [6] are systematically and considerably larger than the cluster sizes measured in the photometric system of the Crimean Astrophysical Observatory [1] using a broader filter with a width of  $100 \text{ \AA}$ .

Second, a comparison of the equivalent widths  $W_{H\beta}$  (in  $\text{\AA}$ ) quoted in [6] with the fluxes in the  $H\beta$  line [6, Tables 6, 8] unexpectedly shows the brightnesses of all 127 objects calculated using the data of [6] to be same, corresponding to  $24^m$ , which is difficult to imagine. Our measurements of  $m_B$  within the boundaries of the objects given in [6] range from  $16^m$  to  $23^m$ , with the mean being  $19.5^m$ . In our subsequent analysis, we avoided using the equivalent widths  $W_{H\beta}$  from [6].

Third, a comparison of the fluxes in the  $H\beta$  and  $H\alpha$  lines quoted in [6] demonstrates that the ratio  $H\alpha/H\beta$  is systematically and considerably higher than the ratios used in [6] to estimate the extinction occurring in the SFCs of NGC 628. Thus, the interstellar-extinction estimates published in [6] may be systematically low. Belley and Roy [6] could not exclude the possibility that the hydrogen-line fluxes were either overestimated or underestimated, which would result

in underestimated or overestimated extinctions. We consider the extinction in the studied objects in more detail in Section 5 below.

#### 4. COMPARISON OF THE OBSERVED COLORS TO A GRID OF EVOLUTIONARY MODELS

Let us compare the color indices measured for 127 SFCs in Section 2 to the INASAN grid of evolutionary models [16]. The model grid covers a large space of models, and includes 648 evolutionary sequences with various IMFs and evolutionary modes. The IMF parameters vary from 30 to  $120 M_{\odot}$  (with a  $30 M_{\odot}$  increment) for the upper mass limit, and from  $\alpha = -0.35$  to  $\alpha = -4.35$  (increment  $h_{\alpha} = 0.05$ ) for the slope. When  $\alpha = -2.35$ , we have the Salpeter IMF [22]. Two star-formation modes were considered: an instantaneous burst of star formation (IB) and an extended burst of star formation (EB). The age range for the IB models was 1–20 million years and for the EB models 1–100 million years, with the time difference between consecutive models being 0.1 dex (in years). Thus, the model grid consists of 13 284 nodes (5508 IB models, 7776 EB models). We continue to use the INASAN grid of evolutionary models [16] in this study because the available observational data (three color indices, with interstellar extinction unknown) are not sufficient to reveal fine deviations [14, Fig. 1] from more recently published evolutionary models [23, 24].

Figure 2 compares the observed SFC colors in NGC 628 and the INASAN evolution-model grid [16] on a two-color diagram. We can see in Fig. 2a that the observed SFC colors lie to the lower right of the region covered by the model grid, i.e., the color indices are “redder” than those allowed by the theoretical models. We have already mentioned in Section 3 that, in our opinion, the extinction estimates suggested in [6] were systematically low. The SFC positions with their colors corrected using the estimates from [6] likewise do not reach the region covered by the evolutionary model grid (Fig. 2b).

In [14], we analyzed the accuracy of interstellar-extinction estimates using a deviation functional that described the deviations of the observed SFC color indices from the synthetic colors for evolutionary models. Our numerical experiments showed that the INASAN grid of evolutionary models [16] was able to provide very reliable estimates or refinements of the interstellar extinction for a star-forming complex based on the observed colors after undergoing this extinction. The star complex’s chemical composition must be known from independent spectroscopic data. The standard error in the extinction for the selected grid increments in the IMF slope ( $h_{\alpha} = 0.05$ ) and age

( $h_{\log t} = 0.1$ ) is  $\sigma_{A_V} = 0.12^m$ . The uncertainty in the extinction becomes larger when the random errors in the original colors are increased. The standard error for random color errors corresponding to the accuracy of the observed colors is  $\sigma_{A_V} = 0.22^m$ .

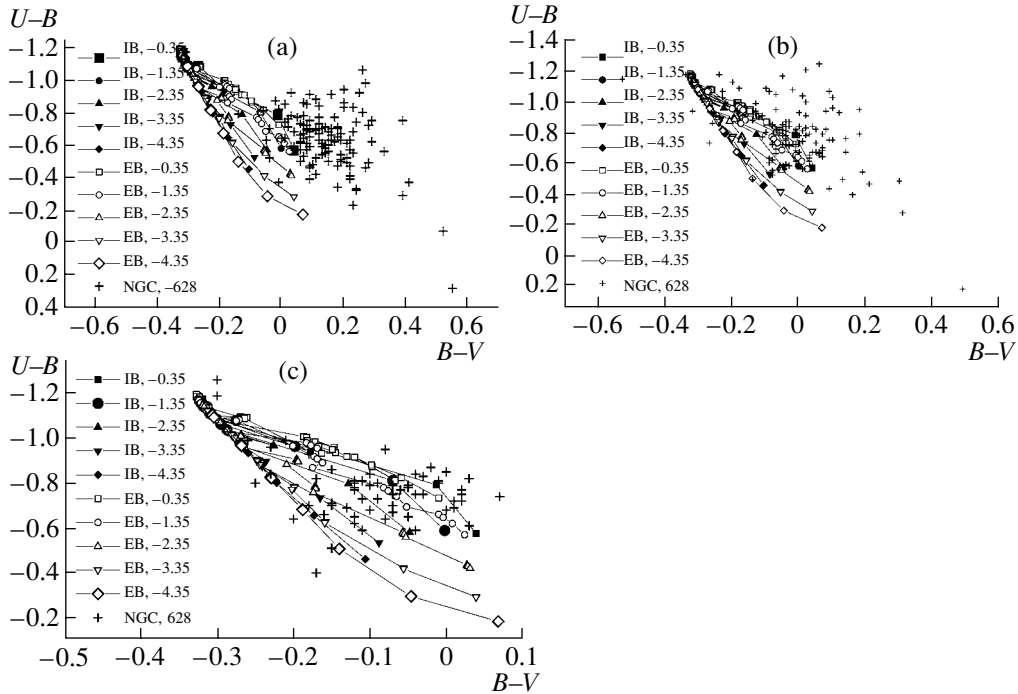
We estimated the extinction by comparing each object’s three observed color indices ( $U-B$ ,  $B-V$ , and  $V-R$ ) to the INASAN grid of evolutionary models [16]. Since the red color indices,  $V-R$ , are in the Cousins ( $V-R$ )<sub>c</sub> system, while the model  $V-R$  colors were calculated in the Johnson ( $V-R$ )<sub>j</sub> system, we used the color-transformation formulas from [25]. For the same reason (the evolutionary model grid was calibrated in the Johnson photometric system [26]), we did not use the ( $R-I$ )<sub>c</sub> color indices we had measured in the Cousins photometric system (see Section 2) for all the HII regions in NGC 628. As described in [14], the  $A_V$  values corresponding to the deepest minimum of the deviation functional have a high correlation ( $r = 98\%$ ) with the initial  $A_V(\text{input})$  values used to “spoil” the test model colors. We adopted the extinction  $A_V$  corresponding to this minimum as the interstellar extinction for each object. Figure 2c shows the positions of the objects relative to the region occupied by the evolutionary models after correcting the observed colors with our  $A_V$  estimates. We can see in Fig. 2c that the objects no longer fall outside the region covered by the evolutionary models by more than the expected uncertainties in the colors. The expected (formal) uncertainty in the extinction is  $\sigma_{A_V} = 0.22^m$ .

The diagrams in Fig. 2 show that, after correcting for interstellar extinction, the studied objects occupy the region covered by the evolutionary model grid. We were able to derive interstellar extinctions,  $A_V$ , for only about half the 124 objects (57 SFCs). It is likely that the real errors in the observed colors for the remaining 60 objects are much larger than the uncertainties formally calculated in Table 2.

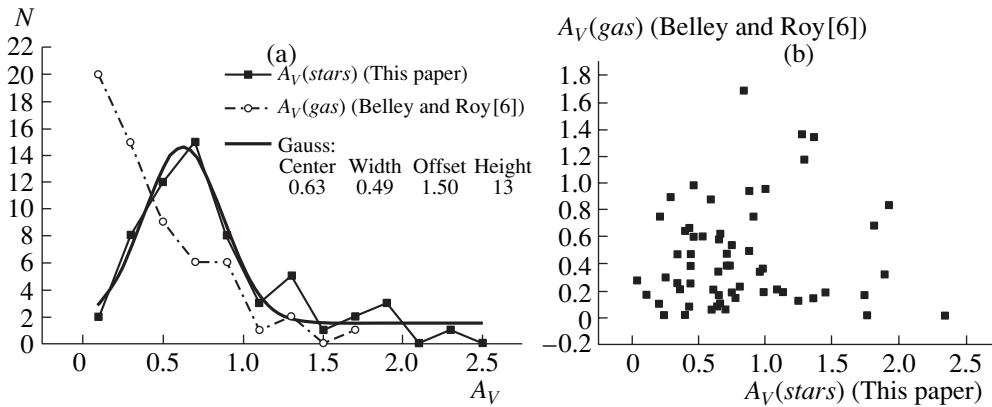
#### 5. EXTINCTION FOR THE SFCs IN NGC 628

Figure 3a shows the distribution of our  $A_V$  estimates for stars in 57 SFCs in NGC 628. The mean value is  $\bar{A}_V = 0.80^m \pm 0.50^m$ . This distribution can be successfully fitted with the Gaussian shown as a solid curve.

The dot–dash broken line in Fig. 3a shows the distribution of extinction estimates for the same objects derived from the Balmer-decrement measurements in Belley and Roy [6]. Although these measurements were made for extinction in an emission line, which should be systematically higher than the extinction for stars [27–30], the estimates in [6] are lower than our  $A_V$  estimates for stellar light by, on average,  $0.35^m$ . The distribution of estimates from [6]



**Fig. 2.** Positions of objects relative to the evolutionary model grid: (a) observed colors, not corrected for interstellar extinction; (b) colors corrected for interstellar extinction using the estimates in [6]; (c) colors corrected for interstellar extinction as derived in this study.



**Fig. 3.** (a) Interstellar-extinction distribution for 57 SFCs in NGC 628; the dot–dash broken line is the distribution for the estimates in Belley and Roy [6]. (b)  $A_V$  estimates from this study (horizontal axis) plotted against the measurements of Belley and Roy [6] (vertical axis).

can be described with a decreasing exponent,  $N = 20.6 \cdot \exp\left(-\frac{A_V - 0.1}{0.5}\right)$ . About half the objects exhibit extinction less than the extinction in the Galaxy towards NGC 628,  $A_V^{Gal} \approx 0.15^m$ .

As noted by Belley and Roy [6], the calibrations they used to calculate the fluxes in the  $H\alpha$  and  $H\beta$  lines can sometimes give systematically overestimated or underestimated values. If we assume that the  $H\alpha$  fluxes were systematically low and the

$H\beta$  fluxes were somewhat too high, the interstellar extinction derived from the Balmer decrement would be systematically underestimated. The uncertainties in the empirical calibrations used in [6] suggest that, in the worst case, the interstellar extinction estimated from the Balmer decrement could be too low or too high by  $\approx 1.5^m$ . Our theoretical extinction estimates for starlight are, on average, higher by  $0.35^m$  than the Balmer interstellar extinctions for emission-line gas measured in [6]. Since the emission-line extinction is

always higher than the stellar-continuum extinction by a factor of 1.3–1.8 [27–30], the estimates of the starlight interstellar extinction for SFCs in [6] will be lower than the theoretical values from our study by, on average,  $0.5^m$ . This difference is well within the systematic deviations due to the calibrations used in [6], and probably provides evidence for systematically overestimated  $H\beta$  fluxes and underestimated  $H\alpha$  fluxes.

Thus, (a) the systematic deviation of the SFC positions with their colors corrected for interstellar extinction using the estimates from [6] on the two-color diagram relative to the region covered by the theoretical model grid (Fig. 2b), (b) the fact that the extinction estimates for starlight are larger than those obtained in [6] from emission lines, and (c) the fact that the extinction in the Galaxy is larger than the measurements in [6] for about half of objects suggest that the SFC extinction estimates given in [6] are systematically low, and should not be used to correct the SFC colors.

The fact that the interstellar-extinction estimates are systematically low by, on average,  $0.5^m$  has virtually no influence on the line-intensity ratios we use to estimate the chemical compositions of the SFCs,  $OIII/H\beta$  and  $NII/H\alpha$ . The relative intensities are too high by less than 1%, since the extinction coefficients differ only slightly for nearby lines. The calibrations have a much larger effect on the  $OIII$  and  $NII$  line fluxes, and can make the abundances too low or too high by  $\Delta_Z = \pm 0.002$ . For the abundance  $Z > 0.020$ , the integrated colors of the star clusters are essentially insensitive to such chemical-composition differences. For the range  $0.010 < Z < 0.017$ , which includes most SFCs in NGC 628, such a systematic abundance bias gives a color-index deviation, for example for  $U - B$ , of  $0.015^m$ , which is within the observational errors. However, since the effect is systematic, the ages can be biased by  $\Delta_{\log t} = \pm 0.04$ , corresponding to a relative age uncertainty of  $\approx 10\%$ . The systematic bias of the interstellar-extinction estimates for this abundance bias is within  $\Delta_{A_V} < 0.005^m$ . Note that these errors can appear in the most unfavorable cases, when the fluxes in the compared lines are biased oppositely by the highest amounts possible for the calibrations used in [6].

Closing this section, we conclude that the flux-calibration uncertainties in [6] prevented the derivation of reliable interstellar extinctions for the SFCs in NGC 628, but did not hinder satisfactory estimation of the chemical abundances for these objects.

## 6. THE AGE–EXTINCTION AMBIGUITY

When comparing the observed colors to those for evolutionary models of star clusters in the presence

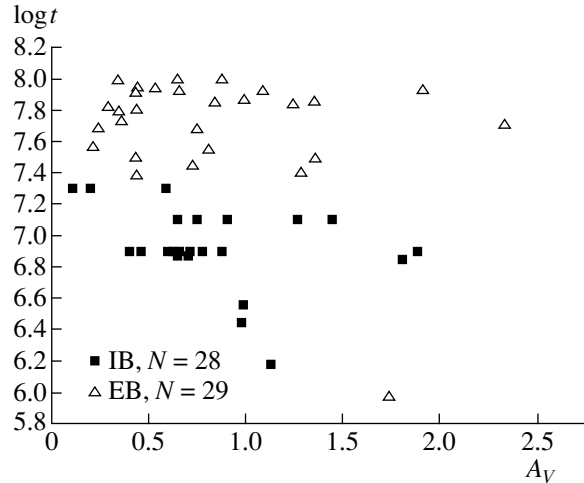


Fig. 4. Age–extinction diagram for 57 SFCs in NGC 628.

of interstellar extinction,  $A_V$ , that is not known from independent observations, we can encounter the so called age–extinction degeneracy: interstellar extinction can be underestimated due to overestimation of the cluster ages and vice versa. In both cases, the age–extinction diagram will show a correlation between these parameters. The uncertainty in the parameters increases when there are fewer observed values or a larger number of model parameters to be determined. The uncertainty also increases if the grid of evolutionary models is sparser. In practice, with only one to three evolutionary sequences and two color indices, we will always have to deal with the age–extinction ambiguity; however, our numerical experiment indicated that the extinctions and ages were determined fairly accurately, and that the age–extinction degeneracy was small or absent. Thus, we expect the level of the age–extinction ambiguity to be low. To test the influence of this ambiguity on the results, we plotted an age ( $t$ ) vs. extinction ( $A_V$ ) diagram for our 57 SFCs (Fig. 4).

Figure 4 demonstrates no correlation between age and extinction for the sample as a whole. For the sample of objects with instantaneous-burst star formation (IB, squares in the diagram), a weak (30%) correlation is present, possibly testifying to a slight age–extinction degeneracy for these objects. The sample of objects with extended-burst star formation (EB, triangles in the diagram) shows nearly no correlation. Thus, our method for deriving the extinctions from three colors and a detailed grid of evolutionary models covering the entire range of IMF parameters and ages makes it possible to lift the age–extinction degeneracy that arises when comparing two colors with only one or a few evolutionary sequences.

Our approach lifts the age–metallicity ambiguity because each object is assigned its own computed grid of evolutionary models that corresponds to the chemical composition derived from independent spectroscopic measurements.

## 7. THE RADIAL EXTINCTION GRADIENT IN NGC 628

Radial chemical-composition gradients in giant HII regions—star-forming complexes—have been revealed in many spiral galaxies (cf. Dutil and Roy [31] and references therein), including NGC 628 [6]. A natural conclusion to draw from the presence of a radial chemical-composition gradient is that chemically enriched SFCs in the inner parts of the galactic disk should show stronger interstellar extinction. Thus, it is of interest to look for radial dependences of the properties of the absorbing matter. Belley and Roy [6] searched for a radial dependence using their interstellar-extinction estimates, but found none. We will attempt to follow the dependence of our estimates, obtained by comparing the observed colors and evolutionary models, on distance to the galactic center (Fig. 5a).

The solid line in Fig. 5a shows the mean slope of the radial gradient of the interstellar extinction for both SFC types (IB and EB). The correlation coefficient for the 54 SFCs located within the corotation radius (dashed line) is  $r = 0.55$ . The correlation coefficient for the entire sample, including SFCs outside the corotation radius, is  $r = 0.50$ . We determined the corotation radius earlier, from a Fourier analysis of the radial-velocity field of NGC 628 [11]. If we separately consider the SFCs with instantaneous (IB) and extended (EB) bursts of star formation, we note in Fig. 5a that the IB SFCs have a shallower gradient (dot–dash line) compared to the EB SFCs (dashed line). Since a radial chemical-composition gradient was found for the SFCs in [6], it is natural to expect a correlation between the extinction  $A_V$  and the abundance  $Z$ . The extinction–abundance diagram in Fig. 5b shows that the EB SFCs exhibit a slope close to 2 (dot–dash line) and the IB SFCs a slope close to unity (dashed line).

## 8. AGE ESTIMATES FOR SFCs IN NGC 628

Our numerical experiment [14] demonstrated that it is possible to get satisfactory age estimates with the three color indices ( $U - B$ ,  $B - V$ ,  $V - R$ ) and metallicities of the SFCs available from observations, with the standard error being  $\sigma_{\log t} = 0.25$ . Let us compare the derived SFC ages with other SFC parameters derived from independent observations: the distances to the galactic center,  $R$ , and abundances,  $Z$ , from [6].

Figure 6a plots age  $t$  vs. galactocentric distance  $R$  diagrams separately for the IB SFCs (squares) and EB SFCs (triangles). No correlation between age and distance from the galactic center is observed for the entire sample of IB and EB SFCs. The ages of the instantaneous-burst SFCs also show no correlation with distance. The ages of the SFCs with extended-burst star formation reveal a negative correlation with distance to the galactic center, although it is weak ( $r = 0.50$ ). Since these objects demonstrated no age–extinction degeneracy (Fig. 4) and the radial gradient for the extinction is itself negative (Fig. 5a), we deduce that the mean age of the EB SFCs decreases from 80 to 40 million years from the galactic center out to the corotation region, with the dispersion being  $\pm 20$  million years. This trend for the EB SFC ages could be due to two physical factors. The first is that the gas density decreases with distance from the galactic center. SFCs with initially lower densities experience a faster dissipation of gas, and the star-forming process ends. Second, the differential rotation is stronger at larger distances from the galactic center, and if a SFC is not gravitationally bound, it will be disrupted. The disruption time near the corotation radius is about 20–30 million years, and could reach hundreds of million of years or more closer to the center, in the zone of rigid-body rotation.

We can see from the age–chemical composition diagram that SFCs with different star-formation modes exhibit opposite trends. The instantaneous-burst SFCs show an anti-correlation between abundance and age: recent bursts have higher chemical abundances than older bursts (the dot–dash line in Fig. 6b). Turning our attention to complexes with extended-burst star formation (EB SFCs, triangles), we see positive correlation between age and abundance. We earlier obtained a similar result for a sample of 100 SFCs in 20 spiral and irregular galaxies [13]. This result also agrees with the conclusion of [32], where it was demonstrated that the ages of star clusters in the LMC, derived in an instantaneous-burst star-formation model, were in anti-correlated with the heavy-element abundances,  $Z$ . However, recall that the correlation between extinction and abundance is positive for the SFCs in NGC 628 (Fig. 5b). Thus, the negative correlation between the ages and abundances of the IB SFCs (squares, dot–dashed line) could partially reflect an age–extinction ambiguity for these objects (Fig. 4). The effects of the age–metallicity ambiguity are eliminated here because the abundance estimates were obtained from independent spectroscopic observations [6].

Note that, near the corotation resonance in Fig. 6a ( $R \approx 7.5$  kpc [11]), both SFC types have approximately equal ages of 20–30 million years, corre-

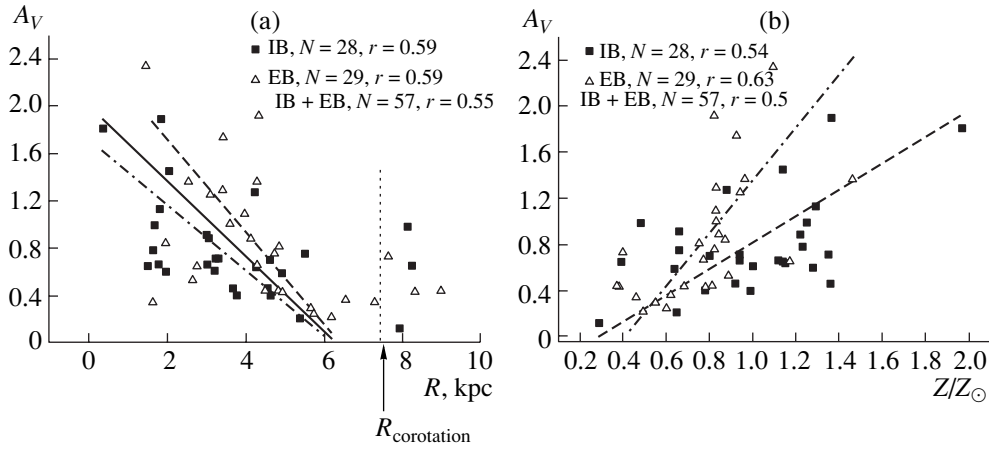


**Fig. 5.** (a) Variations of interstellar extinction for the SFCs in NGC 628 with distance from the galactic center. (b) Extinction–metallicity diagram for the SFCs in NGC 628.

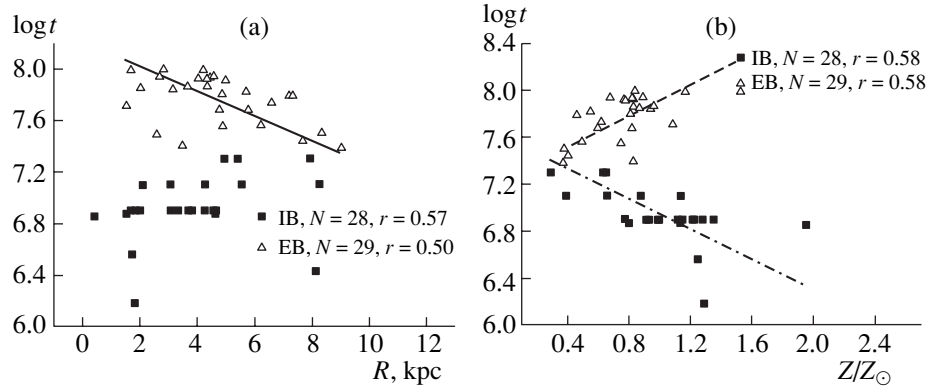


**Fig. 6.** (a) Age  $t$  vs. galactocentric distance  $R$  for SFCs in NGC 628. (b) Age  $t$  vs. abundance  $Z$  for SFCs in NGC 628.

sponding to the ages of the oldest IB SFCs and of relatively young EB SFCs.

## 9. LYMAN-CONTINUUM FLUXES OF THE SFCs IN NGC 628

Our numerical modeling demonstrated that the evolutionary model grid could be used to determine the ratio of the Lyman-continuum luminosity to the  $B$  luminosity,  $\log(N_{\text{LC}}/L_B)$ , with the standard error  $\sigma_{\log(N_{\text{LC}}/L_B)} = 0.22$ .

Let us compare our theoretical estimates to the flux measurements in the  $H\beta$  line from [6] and in the  $H\alpha$  line from [3]. Identifications with the objects from the list of [3] are given in column 3 of Table 2. We measured the  $B$  magnitudes of the star-forming complexes (Table 2), and it is easy to express the observed fluxes,  $F_{H\beta}$  ( $\text{erg cm}^{-2} \text{s}^{-1}$ ) from [6] and  $F_{H\alpha}$  ( $\text{erg cm}^{-2} \text{s}^{-1}$ ) from [3] in terms of the ratio of the Lyman-continuum luminosity to the  $B$  luminosity,  $\log(N_{\text{LC}}/L_B)$ . In these calculations of the luminosity

ratios, we used our extinction-corrected estimates of the SFC magnitudes. The  $H\beta$  fluxes from [6] and  $H\alpha$  fluxes from [3] were also corrected for interstellar extinction, using our estimates in this study. We did not use the equivalent-width estimates,  $W_{H\beta}$ , of [6] because we was demonstrated in Section 3 of this paper that they yielded identical brightnesses  $m_B \approx 24^m$ , for all objects. The observed hydrogen-line fluxes reflect only some fraction of the flux of Lyman photons emitted by cluster stars [15, 33, 34], and the fluxes measured in [3, 6] must be systematically lower than our estimates obtained assuming that all Lyman photons take part in ionizing hydrogen.

Figure 7 compares the difference between our theoretical estimates and the observed magnitudes in [3],  $\Delta_{\text{KH80}} = \log\left(\frac{N_{\text{LC}}}{L_B}\right)_{\text{theor}} - \log\left(\frac{N_{\text{LC}}}{L_B}\right)_{\text{KH80}}$ , and the difference between our theoretical estimates and the observed magnitudes in [6],  $\Delta_{\text{BR92}} = \log\left(\frac{N_{\text{LC}}}{L_B}\right)_{\text{theor}} - \log\left(\frac{N_{\text{LC}}}{L_B}\right)_{\text{BR92}}$ . We can see from Fig. 7 that these

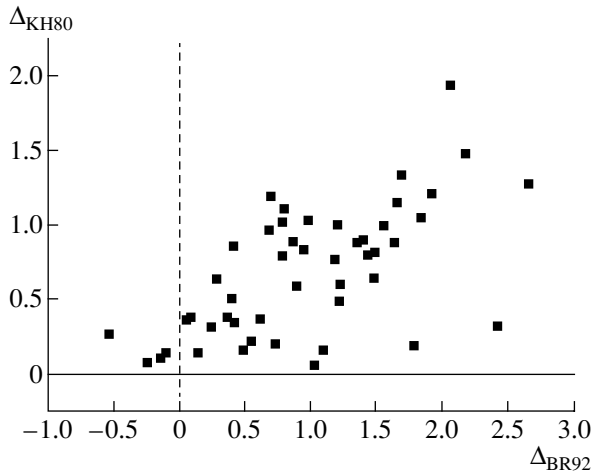


**Fig. 7.** Comparison between calculated and observed fluxes in the Lyman continuum. See text for details.

values are correlated ( $r \approx 0.65$ ), as expected. The expected excess of the theoretical  $N_{LC}/L_B$  ratios compared to the observations can be seen for all the observations of [3] (all the data points are above the solid zero line), but not for all the observations of [6] (four data points are to the left of the dashed zero line).

Recall that the calibrations used in [6] to calculate the emission-line fluxes can lead to their being systematically underestimate or overestimated. Overestimated  $H\beta$  fluxes in [6] would result in overestimated observed  $N_{LC}/L_B$  ratios compared to the theoretical ratios, as is the case for the four SFCs to the left of the dashed zero line in Fig. 7. The extinction measured by Belley and Roy [6] from the Balmer decrement is lower than our estimates (Section 5) based on comparing the SFC colors to a grid of evolutionary models, on average by 0.35 dex. This suggests that the  $H\beta$  fluxes measured in [6] may be too high.

## 10. CONCLUSIONS

In conclusion, we list the main results and conclusions of this study.

(1) We have obtained multicolor *UBVRI* photometry of 127 giant HII regions—star-forming complexes (SFCs) in the galaxy NGC 628 whose chemical compositions had been studied earlier [6]. In addition, we measured the colors of individual parts of multi-component giant SFCs. In total, we measured colors for 229 objects in NGC 628.

(2) We estimated the interstellar extinctions, Lyman-continuum fluxes, and ages for 57 SFCs by comparing our multicolor *UBVR* photometric results for giant HII regions (SFCs) in NGC 628 to the INASAN grid of evolutionary models.

(3) We detected a negative gradient of the extinction in the SFCs in the radial direction, and a positive

correlation between extinction and chemical abundance in the SFCs, equivalent to the radial chemical-composition gradient earlier reported in [6]. In this connection, it would be interesting to obtain new spectroscopy of these SFCs to compare the interstellar extinctions predicted based on the multicolor photometry to the measured values derived from the Balmer decrements.

(4) We confirm the correlations between age and chemical composition for the SFCs reported earlier. The effects of the age–metallicity ambiguity are negligible for our data, since the chemical compositions were derived from independent spectroscopic data.

## ACKNOWLEDGMENTS

The authors thank A.E. Piskunov (INASAN) for discussions of evolutionary models for star clusters. This study was supported by the Russian Foundation for Basic Research (project codes 04-02-16518, 05-02-16454, and 06-02-16857). F.Kh.S. expresses his gratitude to ALDI Einkauf GmbH (Germany) for financial support.

## REFERENCES

1. I. I. Pronik and K. K. Chuvaev, *Izv. Krym. Astrofiz. Obs.* **38**, 219 (1967).
2. G. Natali, F. Pedichini, and M. Righini, *Astron. Astrophys.* **256**, 79 (1992).
3. R. C. Kennicutt and P. W. Hodge, *Astrophys. J.* **241**, 573 (1980).
4. G. S. Shostak and P. C. van der Kruit, *Astron. Astrophys.* **132**, 20 (1984).
5. J. Kamphuis and F. Briggs, *Astron. Astrophys.* **253**, 335 (1992).
6. J. Belley and J.-R. Roy, *Astrophys. J., Suppl. Ser.* **78**, 61 (1992).
7. A. Sandage and G. A. Tammann, *Astrophys. J.* **190**, 525 (1974).
8. G. Vaucoulers, A. Vaucoulers, and H. G. Corwin, *Second Reference Catalog of Bright Galaxies* (University of Texas, Austin, 1976).
9. E. Holmberg, *Medd. Lund. Astron. Obs., Ser. II* **136** (1958).
10. M. L. McCall, P. M. Rybski, and G. A. Shields, *Astrophys. J., Suppl. Ser.* **57**, 1 (1985).
11. F. Kh. Sakhilov and M. A. Smirnov, *Astron. Zh.* **81**, 1093 (2004) [*Astron. Rep.* **48**, 995 (2004)].
12. F. Sakhilov and M. A. Smirnov, *Astron. Astrophys.* **354**, 802 (2000).
13. F. Kh. Sakhilov and M. A. Smirnov, *Astron. Zh.* **78**, 3 (2001) [*Astron. Rep.* **45**, 1 (2001)].
14. A. S. Gusev, V. I. Myakutin, F. Kh. Sakhilov, and M. A. Smirnov, *Astron. Zh.* **84** (2007) (in press).
15. F. Kh. Sakhilov and M. A. Smirnov, *Astron. Zh.* **81**, 998 (2004) [*Astron. Rep.* **48**, 909 (2004)].
16. A. E. Piskunov and V. I. Myakutin, *Astron. Zh.* **73**, 520 (1996) [*Astron. Rep.* **40**, 472 (1996)].

17. B. P. Artamonov, Yu. Yu. Badan, V. V. Bruevich, and A. S. Gusev, *Astron. Zh.* **76**, 438 (1999)[*Astron. Rep.* **43**, 377 (1999)].
18. A. U. Landolt, *Astron. J.* **104**, 340 (1992).
19. A. S. Gusev, *Astron. Zh.* **83**, 195 (2006)[*Astron. Rep.* **50**, 182 (2006)].
20. F. Kh. Sakhibov and M. A. Smirnov, *Astron. Zh.* **67**, 472 (1990)[*Sov. Astron.* **34**, 236 (1990)].
21. M. G. Edmunds and B. E. J. Pagel, *Mon. Not. R. Astron. Soc.* **211**, 507 (1984).
22. E. E. Salpeter, *Astrophys. J.* **121**, 161 (1955).
23. Th. Lejeune and D. Schaerer, *Astron. Astrophys.* **366**, 538 (2001).
24. L. Girardi, G. Bertelli, A. Bressan, et al., *Astron. Astrophys.* **391**, 195 (2002).
25. M. S. Bessell, *Publ. Astron. Soc. Pac.* **91**, 589 (1979).
26. H. L. Johnson, *Ann. Rev. Astron. Astrophys.* **4**, 193 (1966).
27. J. Caplan and L. Deharveng, *Astron. Astrophys.* **155**, 297 (1986).
28. F. Kh. Sakhibov and M. A. Smirnov, *Astron. Zh.* **72**, 318 (1995)[*Astron. Rep.* **39**, 281 (1995)].
29. J. Maiz-Apellaniz, J. M. Mas-Hesse, C. Munoz-Tunon, and H. O. Castanede, *Astron. Astrophys.* **329**, 409 (1998).
30. R. Cid Fernandes, A. Mateus, L. Sodre, Jr., et al., *Mon. Not. R. Astron. Soc.* **358**, 363 (2005).
31. Y. Dutil and J.-R. Roy, *Astrophys. J.* **516**, 62 (1999).
32. L. Girardi, C. Chiosi, G. Bertelli, and A. Bressan, *Astron. Astrophys.* **298**, 87 (1995).
33. C. G. Hoopes, S. T. Gottesman, and B. E. Greenwalt, *Astron. J.* **112**, 1429 (1996).
34. M. Rozas, A. Zurita, and J. E. Beckman, *Astron. Astrophys.* **354**, 823 (2000).

*Translated by N. Samus'*